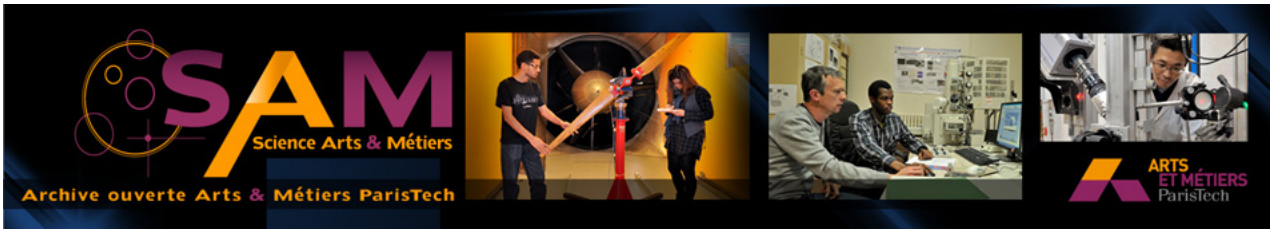

Some features of the PPR cohesive-zone model combined with a linear unloading/reloading relationship

Pierre Gilormini*[a], Julie Diani[b]

[a] *Laboratoire PIMM, ENSAM, CNRS, CNAM, 151 bd de l'Hôpital, 75013 Paris, France*
[b] *LMS, Ecole polytechnique, CNRS, université Paris-Saclay, 91128 Palaiseau, France*

Abstract

A loading/unloading/reloading process is applied to a cohesive zone where the model proposed by Park, Paulino and Roesler in 2009 is combined with a linear unloading/reloading relationship. The applied loading and unloading use the same mixed mode and reloading is in mode I. When the amplitude of preloading is varied, several features are evidenced: jumps of the dissipated energy, reversibility maintained after a traction peak, nonlinear traction variations during unloading, increasing traction during unloading, finite traction after a fracture criterion has been fulfilled, different traction values at the beginning of unloading and when dissipative reloading begins. Moreover, the results depend strongly on the path followed during unloading. Simple modifications of the model allow none of these questionable features to appear.

Keywords: Cohesive zone, PPR model, Loading/unloading relationship

1. Introduction

In 2009, Park, Paulino and Roesler [1] proposed a potential-based cohesive-zone model (CZM) that is very flexible and can cover a large scope of applications. This model has been cited in many papers since then, and programmes were made available to apply the Park-Paulino-Roesler (PPR) model in two-dimensional [2] or three-dimensional [3] finite element simulations. This is one of the noteworthy merits of the model, which should

*Corresponding author. Tel. : + 33 1 44246337; fax: + 33 1 44246190
Email addresses: pierre.gilormini@ensam.eu (Pierre Gilormini*), julie.diani@polytechnique.eu (Julie Diani)

spread its use widely. The PPR model governs the traction-separation relation during loading of the CZM, and it has been shown recently by Park et al. [4] that it does predict a negative tangent stiffness in the softening region along certain loading paths where the CZM model of Camanho et al. [5] that is implemented in the Abaqus code [6] does not, as well as the model of McGarry et al. [7]. Nevertheless, a CZM is of little use when defined for continuous loading only, since unloading and reloading of cohesive zones are likely to happen when complex structures or microstructures containing cohesive zones, like in [8], [9] and [10], for instance, are submitted to general loading conditions. To prevent unphysical reversibility of the CZM, the finite element implementations of [2] and [3] combine the PPR model with a linear unloading/reloading relationship. More recently, Spring et al. [11] noted that the latter formulation may induce undesired self-healing under sinusoidal loading/unloading/reloading, and proposed a rightful thermodynamically consistent formulation to prevent the unphysical response of the model. The purpose of this paper is to further expand and explain the list of questionable features (including energy jumps) that may appear when formulation [2] or [3] is used, and to show that the reformulation [11] prevents them. This is all the more important for formulations [2] and [3] are openly available as Abaqus user element routines, and therefore they are already in use and likely continue to spread among the community.

In what follows, the original PPR model is recalled first, with emphasis put on some aspects that are important for the subsequent analysis. Attention is restricted to the PPR model of 2009, which does not include the variant of Spring and Paulino [9], where friction was added, or the extrinsic version of the model [1]. Moreover, this model is combined with a linear unloading/reloading relationship, like in the programmes given in [2] and [3]. For comparison purposes, the reformulation of Spring et al. [11] is also recalled briefly. The rest of the paper focuses on the application of the model and its reformulation to essentially a mixed-mode proportional loading followed by proportional unloading and finally by mode I reloading.

2. The models considered

Consider a separation vector $\overrightarrow{\Delta}$ in a cohesive zone, with a normal component $\Delta_{\mathrm{n}} = \overrightarrow{\Delta}.\overrightarrow{n}$ and a tangential component $\Delta_{\mathrm{t}} = \sqrt{\overrightarrow{\Delta}.\overrightarrow{\Delta} - \Delta_{\mathrm{n}}^2}$. The case of negative Δ_{n} values, for which an elastic response applies, is not considered here to keep things simple, and therefore Δ_{n} is assumed positive in what follows. The original PPR model of [1] as well as its reformulation by

Spring et al. [11] can be stated simply from the following functions

$$f_{\mathrm{n}}(\Delta_{\mathrm{n}}) = \left(\frac{\alpha}{m}\right)^m \left(1 - \frac{\Delta_{\mathrm{n}}}{\delta_{\mathrm{n}}}\right)^\alpha \left(\frac{m}{\alpha} + \frac{\Delta_{\mathrm{n}}}{\delta_{\mathrm{n}}}\right)^m \quad \text{and}$$
$$f_{\mathrm{t}}(\Delta_{\mathrm{t}}) = -\phi_{\mathrm{t}} \left(\frac{\beta}{n}\right)^n \left(1 - \frac{\Delta_{\mathrm{t}}}{\delta_{\mathrm{t}}}\right)^\beta \left(\frac{n}{\beta} + \frac{\Delta_{\mathrm{t}}}{\delta_{\mathrm{t}}}\right)^n + \phi_{\mathrm{t}} - \phi_{\mathrm{n}} \quad (1)$$

if the mode II fracture energy ϕ_{t} is larger than the mode I fracture energy ϕ_{n}, or

$$f_{\mathrm{n}}(\Delta_{\mathrm{n}}) = -\phi_{\mathrm{n}} \left(\frac{\alpha}{m}\right)^m \left(1 - \frac{\Delta_{\mathrm{n}}}{\delta_{\mathrm{n}}}\right)^\alpha \left(\frac{m}{\alpha} + \frac{\Delta_{\mathrm{n}}}{\delta_{\mathrm{n}}}\right)^m + \phi_{\mathrm{n}} - \phi_{\mathrm{t}}$$
$$\text{and} \quad f_{\mathrm{t}}(\Delta_{\mathrm{t}}) = \left(\frac{\beta}{n}\right)^n \left(1 - \frac{\Delta_{\mathrm{t}}}{\delta_{\mathrm{t}}}\right)^\beta \left(\frac{n}{\beta} + \frac{\Delta_{\mathrm{t}}}{\delta_{\mathrm{t}}}\right)^n \quad (2)$$

otherwise (including the case where $\phi_{\mathrm{t}} = \phi_{\mathrm{n}}$). In addition to the fracture energies ϕ_{n} and ϕ_{t}, six parameters are involved in the model: the normal and tangential cohesive strengths ($\sigma_{\max}$ and $\tau_{\max}$), the shape exponents $\alpha \geq 1$ and $\beta \geq 1$, and the ratios λ_{n} and λ_{t} between 0 and 1. From these eight parameters, the following quantities can be deduced, which are used in (1) and (2):

$$m = \frac{\alpha(\alpha-1)\lambda_{\mathrm{n}}^2}{1-\alpha\lambda_{\mathrm{n}}^2} \qquad \text{and} \qquad n = \frac{\beta(\beta-1)\lambda_{\mathrm{t}}^2}{1-\beta\lambda_{\mathrm{t}}^2} \quad (3)$$

as well as the normal and tangential separation lengths for mode I and mode II fractures, respectively:

$$\delta_{\mathrm{n}} = \frac{\phi_{\mathrm{n}}}{\sigma_{\max}} \alpha\lambda_{\mathrm{n}}(1-\lambda_{\mathrm{n}})^{\alpha-1} \left(1 + \frac{\alpha}{m}\right) \left(1 + \lambda_{\mathrm{n}}\frac{\alpha}{m}\right)^{m-1} \quad \text{and}$$
$$\delta_{\mathrm{t}} = \frac{\phi_{\mathrm{t}}}{\tau_{\max}} \beta\lambda_{\mathrm{t}}(1-\lambda_{\mathrm{t}})^{\beta-1} \left(1 + \frac{\beta}{n}\right) \left(1 + \lambda_{\mathrm{t}}\frac{\beta}{n}\right)^{n-1}. \quad (4)$$

With $f'_{\mathrm{n}}(\Delta_{\mathrm{n}})$ and $f'_{\mathrm{t}}(\Delta_{\mathrm{t}})$ denoting the first derivatives of $f_{\mathrm{n}}(\Delta_{\mathrm{n}})$ and $f_{\mathrm{t}}(\Delta_{\mathrm{t}})$, respectively, the normal and tangent traction components write as follows in the original PPR model:

$$T_{\mathrm{n}} = f'_{\mathrm{n}}(\Delta_{\mathrm{n}})\, f_{\mathrm{t}}(\Delta_{\mathrm{t}}) \qquad \text{and} \qquad T_{\mathrm{t}} = f'_{\mathrm{t}}(\Delta_{\mathrm{t}})\, f_{\mathrm{n}}(\Delta_{\mathrm{n}}) \quad (5)$$

provided that no fracture has occurred yet and that no unloading or partial reloading applies. The fracture conditions are given by the normal traction T_{n} or the tangential traction T_{t} reaching a zero value for a non-zero separation. When one of these conditions applies, the corresponding traction

component stays zero for further loadings. Therefore, four cases apply: no fracture has occurred yet, the cohesive zone has lost its stiffness for normal separation but not yet for tangential separation, it has lost its stiffness for tangential separation but not yet for normal separation, or any load bearing capacity is lost (both T_n and T_t have reached a zero value). According to (5), the zero stiffness condition for normal separation is obtained when either $f'_\mathrm{n}(\Delta_\mathrm{n}) = 0$ or $f_\mathrm{t}(\Delta_\mathrm{t}) = 0$, which occurs for either $\Delta_\mathrm{n} = \delta_\mathrm{n}$ or for $\Delta_\mathrm{t} = \delta_\mathrm{t}$ if $\phi_\mathrm{t} \leq \phi_\mathrm{n}$ or for $\Delta_\mathrm{t} = \overline{\delta}_\mathrm{t}$ if $\phi_\mathrm{t} > \phi_\mathrm{n}$, where $\overline{\delta}_\mathrm{t}$ is the single root of $f_\mathrm{t}(\overline{\delta}_\mathrm{t}) = 0$ between 0 and δ_t [1]. Similarly, the zero stiffness condition for tangential separation is obtained when either $\Delta_\mathrm{t} = \delta_\mathrm{t}$ or for $\Delta_\mathrm{n} = \delta_\mathrm{n}$ if $\phi_\mathrm{t} > \phi_\mathrm{n}$ or for $\Delta_\mathrm{n} = \overline{\delta}_\mathrm{n}$ if $\phi_\mathrm{t} \leq \phi_\mathrm{n}$, where $\overline{\delta}_\mathrm{n}$ is the single root of $f_\mathrm{n}(\overline{\delta}_\mathrm{n}) = 0$ between 0 and δ_n. Accordingly, it may be noted that the load bearing capacity of the cohesive zone for normal (resp. tangential) separation can be zeroed by a purely tangential (resp. normal) loading of sufficient magnitude. It can also be checked that the energy dissipated during a purely normal (resp. tangential) and continuously increasing separation is equal to ϕ_n (resp. ϕ_t) when the fracture condition is met, which confirms the physical interpretation of δ_n (resp. δ_t) as the separation length for mode I (resp. mode II) fracture.

In addition to lost load bearing capacities, the other cases where (5) does not apply are unloading and partial reloading. In the implementations given in [2] and [3], these cases are controlled by two state variables $\Delta_\mathrm{n}^\mathrm{max}$ and $\Delta_\mathrm{t}^\mathrm{max}$, which are the largest values of Δ_n and Δ_t reached so far, keeping $\Delta_\mathrm{n}^\mathrm{max} = 0$ (resp. $\Delta_\mathrm{t}^\mathrm{max} = 0$) as long as $\Delta_\mathrm{n} < \delta_\mathrm{n}^\mathrm{peak}$ (resp. $\Delta_\mathrm{t} < \delta_\mathrm{t}^\mathrm{peak}$), with $\delta_\mathrm{n}^\mathrm{peak} = \lambda_\mathrm{n}\delta_\mathrm{n}$ (resp. $\delta_\mathrm{t}^\mathrm{peak} = \lambda_\mathrm{t}\delta_\mathrm{t}$). Unloading corresponds to decreasing Δ_n and Δ_t, and partial reloading to increasing values lower than $\Delta_\mathrm{n}^\mathrm{max}$ and $\Delta_\mathrm{t}^\mathrm{max}$. Park and Paulino [2] proposed a nonlinear unloading/reloading response that involves two additional shape parameters, which are not used in their implementation actually. Therefore, a linear response to the origin is considered here, which is considered frequently in CZMs ([12], [13], [8], for instance) and is implemented in the programmes given in [2] and [3]. According to [2], the traction components are given by

$$T_\mathrm{n} = f'_\mathrm{n}(\Delta_\mathrm{n}^\mathrm{max})\, f_\mathrm{t}(\Delta_\mathrm{t})\frac{\Delta_\mathrm{n}}{\Delta_\mathrm{n}^\mathrm{max}} \quad \text{and} \quad T_\mathrm{t} = f'_\mathrm{t}(\Delta_\mathrm{t}^\mathrm{max})\, f_\mathrm{n}(\Delta_\mathrm{n})\frac{\Delta_\mathrm{t}}{\Delta_\mathrm{t}^\mathrm{max}} \tag{6}$$

instead of (5) for unloading or partial reloading of the normal (resp. tangential) component when $\Delta_\mathrm{n}^\mathrm{max} \geq \delta_\mathrm{n}^\mathrm{peak}$ (resp. $\Delta_\mathrm{t}^\mathrm{max} \geq \delta_\mathrm{t}^\mathrm{peak}$). When the parameters of the next section are used, Figure 1 illustrates this response for the normal traction as a straight dashed line, whereas the solid curve shows the response that applies for a continuously increasing normal separation. The maximum of this curve gives the interpretation of σ_max as the peak

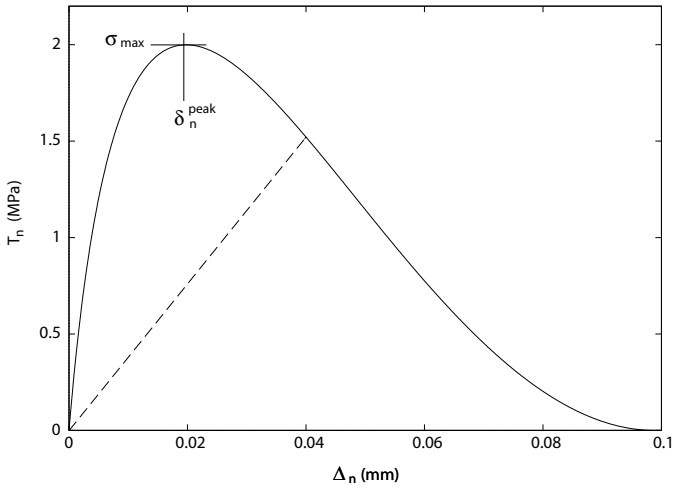

Figure 1: Normal traction induced in mode I when separation increases continuously (solid line) or during unloading/reloading after a separation of 0.04 mm has been applied (dashed line). The parameter values of section 3 were used.

normal traction in mode I and of $\delta_{\rm n}^{\rm peak}$ as the separation that leads to this maximum. Note that (5) applies, and the curve is followed, during unloading and reloading as long as the peak has not been passed: the response is elastic, but not linear elastic, up to the softening region.

In short, the reformulation of [11] involves two modifications of the above model. First, the state variables $\Delta_{\rm n}^{\rm max}$ and $\Delta_{\rm t}^{\rm max}$ are updated as soon as $\Delta_{\rm n} > 0$ and $\Delta_{\rm t} > 0$. Thus, $\delta_{\rm n}^{\rm peak}$ and $\delta_{\rm t}^{\rm peak}$ are not used, and the linear unloading/reloading response applies even before any peak has been passed. The second modification affects the traction components, which are given by:

$$T_{\rm n} = f'_{\rm n}(\Delta_{\rm n}^{\rm max})\, f_{\rm t}(\Delta_{\rm t}^{\rm max}) \frac{\Delta_{\rm n}}{\Delta_{\rm n}^{\rm max}} \quad \text{and} \quad T_{\rm t} = f'_{\rm t}(\Delta_{\rm t}^{\rm max})\, f_{\rm n}(\Delta_{\rm n}^{\rm max}) \frac{\Delta_{\rm t}}{\Delta_{\rm t}^{\rm max}} \quad (7)$$

where the ratio $\Delta_{\rm n}/\Delta_{\rm n}^{\rm max}$ (resp. $\Delta_{\rm t}/\Delta_{\rm t}^{\rm max}$) should be omitted if $\Delta_{\rm n}^{\rm max} = 0$ (resp. $\Delta_{\rm t}^{\rm max} = 0$). The latter condition is not included explicitly by Spring et al. [11] but is necessary to avoid indeterminate 0/0 ratios. Equations (7) apply for loading as well as for unloading/reloading, and the same fracture conditions as for the original PPR model are used. These two modifications are easily implemented in the Fortran programmes of [2] (for 2D finite element simulations) and [3] (for 3D simulations). In these programmes, the tangent matrix is also required, which involves the derivatives of $T_{\rm n}$ and $T_{\rm t}$

with respect to Δ_n and Δ_t, where it should be kept in mind that the derivative of Δ_n^{max} (resp. Δ_t^{max}) is either 1 (if $\Delta_n = \Delta_n^{max}$, resp. $\Delta_t = \Delta_t^{max}$) or 0 (if $\Delta_n < \Delta_n^{max}$, resp. $\Delta_t < \Delta_t^{max}$). This has been applied in [11], where the various cases that apply to the tangent matrix are detailed. However, the tangent matrix is not required to perform the computations presented below.

3. Application

The following set of parameters is used: $\phi_n = 100$ J/m^2, $\phi_t = 300$ J/m^2, $\sigma_{max} = 2$ MPa, $\tau_{max} = 4$ MPa, $\alpha = 3$, $\beta = 5$, $\lambda_n = 0.20$, and $\lambda_t = 0.25$. The λ_n and λ_t values are quite large in order to make some effects more apparent, but no restriction is given a priori between the bounds 0 and 1 for the applicability of the PPR model, even though λ_n and λ_t are frequently taken small and related to numerical stability. By the way, λ_n and λ_t values of 0.1 or 0.2 were used in the tests performed by Park et al. [4] and Spring et al. [11]. More generally, one of the merits of the PPR model is its flexibility due to the large possibilities offered by eight parameters, and it seems very difficult to restrict their ranges so as to avoid all the features evidenced below.

Since $\phi_t > \phi_n$, (1) applies, and the following useful values are obtained: $m = 0.273$, $n = 1.818$, $\delta_n = 0.099$ mm, $\delta_t = 0.171$ mm, $\overline{\delta}_t = 0.039$ mm, $\delta_n^{peak} = 0.020$ mm, and $\delta_t^{peak} = 0.043$ mm. The applied loading consists in (i) a proportional mixed-mode loading where $\Delta_t = \Delta_n$ up to a predefined Δ value, (ii) a proportional mixed-mode unloading where $\Delta_t = \Delta_n$ down to 0, and (iii) a mode I reloading (keeping $\Delta_t = 0$) up to $\Delta_n > \delta_n$. In addition, proportional loading will be followed by various unloading paths in one case.

Figure 2 shows how the energy that is dissipated in the whole loading process varies when the amplitude of the proportional loading increases, for the original model as well as for the modified model. It may be noted first that the two models give quite different energy values. In the range of proportional loading amplitudes Δ considered, the dissipated energy given by the original model has a plateau at both low and high proportional loading amplitudes, with the first plateau being equal to the mode I fracture energy of $\phi_n = 100$ J/m^2, whereas the modified model exhibits one at large values only, where both models coincide. Another evident feature of the original model is a set of three discontinuities, at $\Delta = \delta_n^{peak} = 0.020$ mm, $\Delta = \delta_t^{peak} = 0.043$ mm, and $\Delta = \delta_n = 0.099$ mm, whereas the modified model gives a smooth continuous curve with a slope jump at $\Delta = \overline{\delta}_t = 0.039$ mm. These

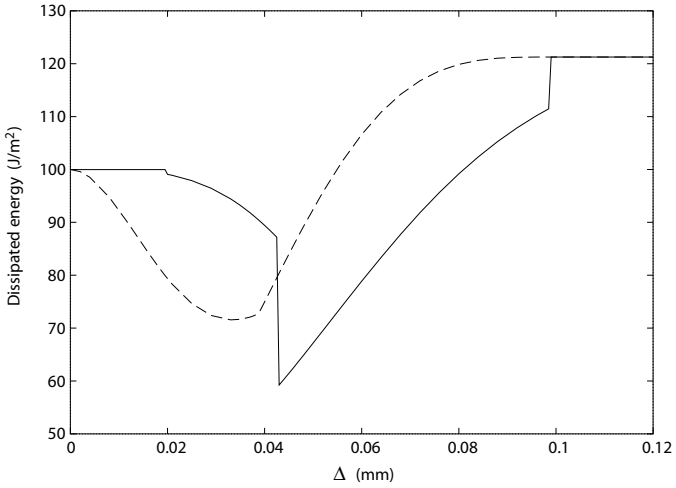

Figure 2: Energy that is dissipated in the process of proportional loading/unloading and mode I reloading, when the amplitude of the proportional loading varies. Original model (solid line) and modified model (dashed line).

differences are explained below by analyzing the variations of the traction components during the loading process.

First, consider proportional loading amplitudes Δ around $\delta_{\mathrm{n}}^{\mathrm{peak}} = 0.020$ mm. As expected, Figure 3a shows that during unloading both traction values back up along the same curves that they followed during loading when Δ_{n} and Δ_{t} reached 0.019 mm, below $\delta_{\mathrm{n}}^{\mathrm{peak}}$ and $\delta_{\mathrm{t}}^{\mathrm{peak}}$, respectively. It may be noted that the T_{n} unloading curve has a peak, and this consolidation (increasing traction) during an unloading process (decreasing displacement) may surprise. This is comparable to the traction fluctuations evidenced by Park et al. [4], but here in the elastic region of the PPR model, whereas the fluctuations noticed in [4] appeared in the softening regions of the models of Camanho et al. [5] and McGarry et al. [7]. Recalling that an elastic, reversible, behavior applies in pure mode I (Figure 1) or mode II up to the peak but not beyond, the fact that a peak may be passed during mixed-mode loading while reversibility is maintained lessens the physical meaning of peaks in this model. As a consequence of reversibility during proportional loading/unloading, the same solid curve as in Figure 1 is followed during mode I reloading, and the final dissipated energy when $\Delta_{\mathrm{n}} = \delta_{\mathrm{n}}$ is equal to $\phi_{\mathrm{n}} = 100$ J/m^2. In contrast, both unloading curves follow straight lines with the modified model (Figure 3b) because no peak value is used to start

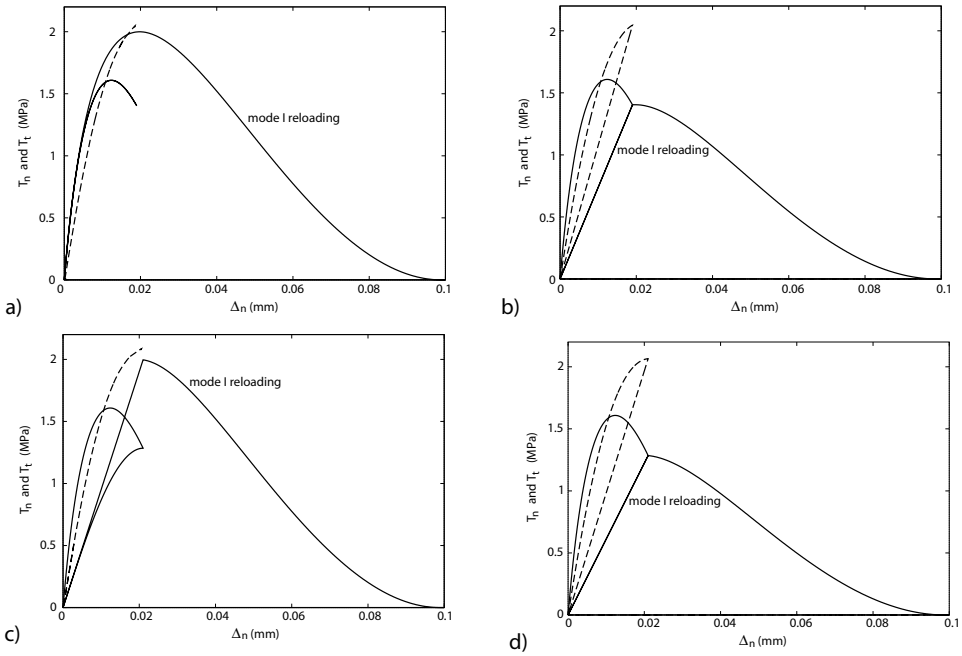

Figure 3: Variations of the traction components T_n (solid lines) and T_t (dashed lines) during the process of proportional loading/unloading and mode I reloading, for a proportional loading amplitude of $\Delta = 0.019$ mm, (a) and (b), or $\Delta = 0.021$ mm, (c) and (d). Original model on the left, modified model on the right.

using the linear response. The reloading curve reaches the final proportional loading point, where it kinks, and then decreases up to mode I fracture. As can be observed directly from the area below the curves, the total dissipated energy (80.5 J/m^2) is lower than ϕ_n. Thus, Figure 3a and b explain why the energy dissipated by the original model has a plateau up to $\Delta = \delta_\mathrm{n}^\mathrm{peak}$ and why the modified model gives lower values.

When proportional loading is applied up to $\Delta = 0.021$ mm, the $\delta_\mathrm{n}^\mathrm{peak}$ value is exceeded, and therefore the unloading curve for T_n obeys (6). Since Δ_t varies during proportional unloading, (6) indicates that T_n does not vary linearly, as can be observed in Figure 3c. This illustrates that the unloading/reloading relationship used is linear for pure mode I (Figure 1, for instance) or mode II, but not for mixed modes. Figure 3c also shows that the energy that is dissipated during the proportional loading/proportional unloading process jumps from 0 (Figure 3a) to a finite value (equal to the surface between the loading/unloading curves for T_n in Figure 3c, since T_t

is reversible) when the $\delta_{\mathrm{n}}^{\mathrm{peak}}$ value is crossed. Such an energy discontinuity is inherent to any CZM model that obeys a curved line in the reversible range and an unloading straight line when irreversibility has appeared. In the case of mode I, for instance, this energy jump can be visualized easily in Figure 1 by shifting the end of the dashed line to the peak of the curve. As can be observed in Figure 3c, mode I reloading adds a significant amount of dissipated energy and the final value (98.9 J/m^2) is close to the plateau, which leads to a small energy jump in Figure 2. Note also that the kink point of the curve for T_{n} during mode I reloading, which starts with a straight segment, differs from the final proportional loading point. This difference is not observed when the modified model is used (Figure 3d), where the dissipated energy varies continuously (compare Figures 3b and d).

Consider now proportional loading amplitudes Δ around $\overline{\delta}_{\mathrm{t}} = 0.039$ mm. Figure 4a, for $\Delta = 0.038$ mm, shows the same effects as Figure 3c, but enhanced significantly and with a peak for T_{t} being overpassed largely in a reversible manner. The difference between the turning point at proportional unloading and the kink point at reloading is very large, with the former corresponding to a very low T_{n} value. Such large tractions reached in mode I are quite unexpected after the condition for losing load bearing capacity for normal separation has been almost reached. Moreover, T_{n} increases significantly during unloading and follows a strongly nonlinear curve. A similar feature can be observed for the T_{t} component in Figure 9b of [11] during a sinusoidal loading history. None of these effects is observed with the modified model (Figure 4b below and Figure 9c of [11]). The proportional loading applied in Figure 4c is such that Δ_{n}, which is 0.041 mm, exceeds $\overline{\delta}_{\mathrm{t}}$. Since this is a fracture condition for normal separation, zero T_{n} values are obtained but $\Delta_{\mathrm{t}}^{\max}$ is still zero because Δ_{t} (0.038 mm) has not reached $\delta_{\mathrm{t}}^{\mathrm{peak}}$ (0.043 mm) yet. Consequently, (5) applies during unloading and T_{n} takes positive values that are very questionable after load bearing capacity for normal separation has been lost in principle. For the same reason, quite large positive T_{n} values are also obtained during mode I reloading, as shown in Figure 4c. Of course, this very special feature is obtained here because the parameters have been chosen such that $\overline{\delta}_{\mathrm{t}} < \delta_{\mathrm{t}}^{\mathrm{peak}}$. It is not limited to mixed-mode loading, as can be checked very simply by applying $\Delta_{\mathrm{t}} = \overline{\delta}_{\mathrm{t}}$ in mode II, unload, and then reload in mode I. This paradox disappears for a slightly larger Δ value of 0.044 mm (Figure 4e), T_{n} remains zero during unloading and reloading, but energy is now dissipated by T_{t} during proportional unloading, which induces a jump in Figure 2. The traction variations in Figure 4e are similar to what is given by the modified model (except

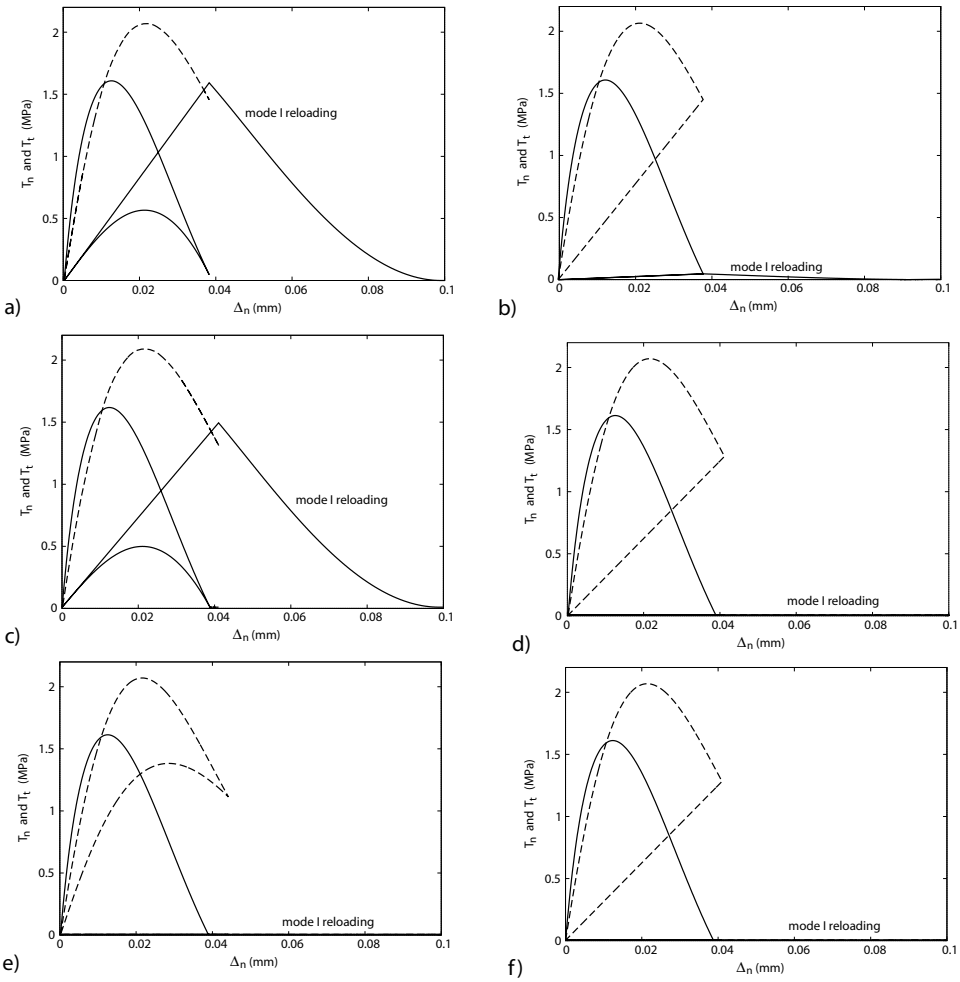

Figure 4: Variations of the traction components T_{n} (solid lines) and T_{t} (dashed lines) during the process of proportional loading/unloading and mode I reloading, for a proportional loading amplitude of $\Delta = 0.038$ mm, (a) and (b), or $\Delta = 0.041$ mm, (c) and (d), or $\Delta = 0.044$ mm, (e) and (f). Original model on the left, modified model on the right.

for T_t during unloading). The latter followed a smooth evolution through Figures 4b, d, and e, with disappearance of the dissipated energy during reloading (see bottom of Figure 4b) when $\Delta = \overline{\delta}_\mathrm{t}$ explaining the kink shown by the modified model in Figure 2.

Another typical feature of the original model is demonstrated in Figure 5, showing the variations of T_t vs. Δ_t, where a proportional loading up to $\Delta = 0.044$ mm is applied and is followed by one of three different unloading paths. The first unloading path is proportional (with $\Delta_\mathrm{t} = \Delta_\mathrm{n}$), like in Figure 4e, the second consists in decreasing Δ_n to 0 while keeping Δ_t constant and then decreasing Δ_t to 0 (normal/tangential unloading), and the third unloading path decreases Δ_t before Δ_n (tangential/normal unloading). As expected, the two sequential unloading paths lead to linear variations of the T_t traction component (and also of the T_n component, not shown), since they do not involve mixed modes but mode I and mode II only. Figure 5 clearly shows that changing the unloading path affects the traction variations significantly. Consistently, the energy that is dissipated along the loading/unloading closed loop also is different: 60.3 J/m^2 for proportional unloading, 18.7 J/m^2 for the normal/tangential sequence, and 82.2 J/m^2 for the tangential/normal sequence. This dependence on unloading path is another questionable feature of the original model, whereas all three unloading paths lead to the same traction variations with the modified model, which all coincide with the tangential/normal curve displayed in Figure 5, with the same dissipated energy of 82.2 J/m^2 in all three cases. This is a natural consequence of the thermodynamic consistency of the latter model shown by Spring et al. [11]. Similarly, some mode II loading can be applied after proportional loading/unloading, before mode I is applied finally, and this has no effect on the normal traction history when the reformulated model is used, whereas this history is affected (with a lower peak when the mode II amplitude increases) with the original model.

Finally, consider proportional loading amplitudes Δ around $\delta_\mathrm{n} = 0.099$ mm. A loss of load bearing capacity for normal separation takes place during the proportional mixed-mode loading phase because of the large Δ_n value applied, and there remains to examine the evolution of the tangential traction component during the proportional unloading phase. In Figure 6a, $\Delta_\mathrm{n} = 0.098$ mm is imposed, which is slightly below the critical value δ_n that defines one of the conditions for losing load bearing capacity for tangential separation. Therefore, the tangential traction component is slightly above zero at the end of the loading phase and it takes non-zero values during unloading. The latter traction variations correspond to the T_t term given in (6), which does not tend to 0 when $\Delta_\mathrm{t}^\mathrm{max}$ tends to δ_n and stays below δ_n. The

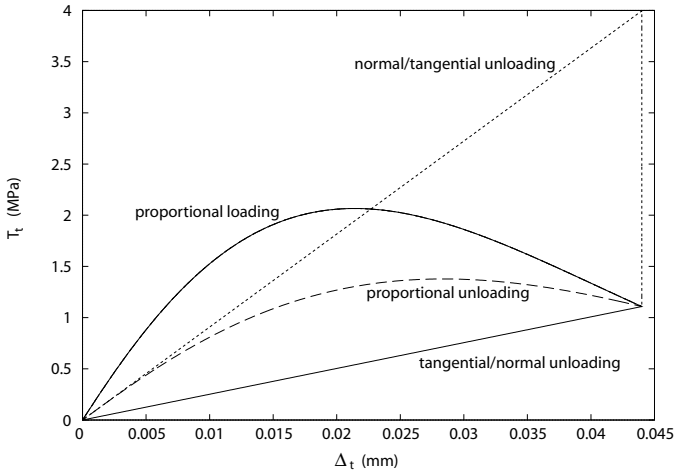

Figure 5: Variations of the traction components T_t given by the original model during a proportional loading up to $\Delta_\mathrm{n} = \Delta_\mathrm{t} = 0.044$ mm (upper solid line) followed by a proportional unloading (dashed line), or by a sequential normal/tangential unloading (dotted line), or by a sequential tangential/normal unloading (lower solid line).

critical value δ_n is exceeded by Δ_n when the proportional amplitude is of 0.1 mm, hence fracture is complete (Figure 6c), which leads to a dissipated energy of 121.3 J/m^2 that corresponds to the final plateau in Figure 2. A jump of the dissipated energy happens before the plateau for $\Delta = \delta_\mathrm{n}$ because the finite T_t values during unloading mentioned above are set to zero all at once when fracture occurs. The same traction variations and dissipated energy are obtained with the modified model for $\Delta = 0.1$ mm, as shown in Figure 6d, and they still apply for larger proportional loading amplitudes, of course. It may be noted eventually that all traction variations obtained during the loading phases in Figures 3, 4, and 6 are parts of the curves shown in Figure 6d.

4. Conclusion

The cohesive-zone model proposed by Park, Paulino and Roesler [1] has been combined with a linear unloading/reloading relationship like in the numerical implementations given in [2] and [3], and a loading/unloading/reloading process has been applied, where loading and unloading used the same proportional mixed mode and reloading was in mode I. Several features could be evidenced when the amplitude of preloading varied: jumps of the

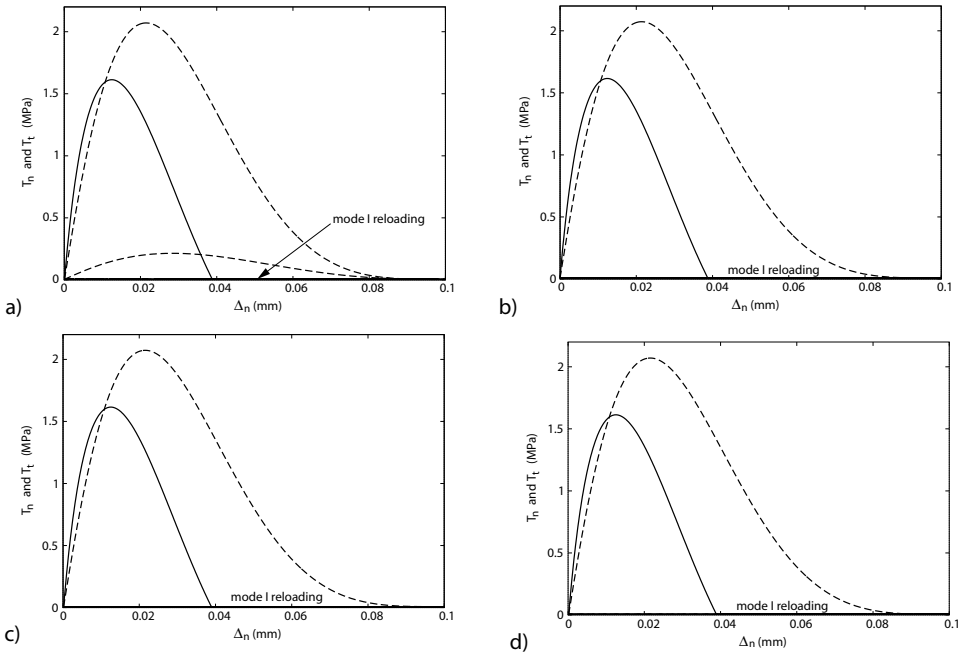

Figure 6: Variations of the traction components T_n (solid lines) and T_t (dashed lines) during the process of proportional loading/unloading and mode I reloading, for a proportional loading amplitude of $\Delta = 0.098$ mm, (a) and (b), or $\Delta = 0.1$ mm, (c) and (d). Original model on the left, modified model on the right.

dissipated energy, reversibility maintained after a traction peak, nonlinear traction variations during unloading, increasing traction during unloading, finite traction after a fracture criterion has been fulfilled, different traction values at the beginning of unloading and when dissipative reloading begins. The results have also been shown to depend strongly on the path followed during unloading. None of these issues appears when the reformulation of Spring et al. [11] is used. Therefore, users of the programmes already available for applying the original model in finite element simulations should be cautious and should check if any of the mentioned features may appear with their sets of parameters, for instance with very small λ_n and λ_t ratios. If this is the case, the programmes should be modified according to the reformulation of [11].

It may be noticed finally that the modified model does not include an initial elastic region, since energy is dissipated by increasing damage from the very beginning of the loading process. In contrast, the original model

defined an elastic region before a softening regime. This involved a peak condition that induced some of the questionable features evidenced here, but an elastic regime may nevertheless be desirable for some users. This might be added to the reformulated, thermodynamically consistent, model.

References

[1] Park K, Paulino GH, Roesler JR. A unified potential-based cohesive model of mixed-mode fracture. J Mech Phys Solids 2009;57:891-908.

[2] Park K, Paulino GH. Computational implementation of the PPR potential-based cohesive model in ABAQUS: Educational perpective. Engng Fract Mech 2012;93:239-262.

[3] Spring DW, Paulino GH. A growing library of three-dimensional cohesive elements for use in ABAQUS. Engng Fract Mech 2014;126:190-216.

[4] Park K, Choi H, Paulino GH. Assessment of cohesive traction-separation relationships in ABAQUS: A comparative study. Mech Res Comm 2016;78:71-78.

[5] Camanho PP, Davila CG, Moura MF. Numerical simulation of mixed-mode progressive delamination in composite materials. J Compos Mater 2003;37:1415-1438.

[6] Abaqus. Version 6.12 Analysis User's Manual, Simulia, Providence, RI; 2012.

[7] McGarry JP, Maírtín ÉÓ, Parry G, Beltz GE. Potential-based and non-potential-based cohesive zone formulations under mixed-mode separation and overclosure. Part I: Theoretical analysis. J Mech Phys Solids 2014;63:336-362.

[8] Segurado J, Llorca J. A new three-dimensional interface finite element to simulate fracture in composites. Int J Solids Struct 2005;41:2977-2993.

[9] Spring DW, Paulino GH. Computational homogenization of the debonding of particle reinforced composites: The role of interphases and interfaces. Comput Mater Sci 2015;109:209-224.

[10] Cerrone A, Wawrzynek P, Nonn A, Paulino GH, Ingraffea A. Implementation and verification of the Park-Paulino-Roesler cohesive zone model in 3D. Engng Fract Mech 2014;120:26-42.

[11] Spring DW, Giraldo-Londoño O, Paulino GH. A Study on the Thermodynamic Consistency of the Park-Paulino-Roesler (PPR) cohesive fracture model. Mech Res Comm 2016;78:100-109.

[12] Tvergaard V. Effect of fibre debonding in a whisker-reinforced metal. Mater Sci Engng 1990;A125:203-213.

[13] Ortiz M, Pandolfi A. Finite-deformation irreversible cohesive elements for three-dimensional crack-propagation analysis. Int J Numer Meth Engng 1999;44:1267-1282.